

Three-dimensional MHD modeling of the solar wind structures associated with 13 December 2006 coronal mass ejection

R. Kataoka,^{1,2} T. Ebisuzaki,¹ K. Kusano,^{3,4} D. Shiota,³ S. Inoue,^{3,5} T. T. Yamamoto,⁴ and M. Tokumaru⁴

Received 17 February 2009; revised 10 June 2009; accepted 24 June 2009; published 6 October 2009.

[1] A 3-D magnetohydrodynamic (MHD) simulation is performed to reconstruct the interplanetary propagation of a coronal mass ejection (CME) that occurred on 13 December 2006. A spheromak-type magnetic field is superposed on a realistic ambient solar wind to reproduce the large-scale interplanetary magnetic field (IMF) associated with the CME. Here we show that a westward and southward directed spheromak CME with reasonable geometric, dynamic, and magnetic parameters reproduces the magnetic cloud, interplanetary shock, and sheath profiles as observed by in situ spacecraft. We suggest that the simple solar wind model developed in this study is topologically complex enough to be consistent with in situ observations, such as southward IMF associated with CMEs.

Citation: Kataoka, R., T. Ebisuzaki, K. Kusano, D. Shiota, S. Inoue, T. T. Yamamoto, and M. Tokumaru (2009), Three-dimensional MHD modeling of the solar wind structures associated with 13 December 2006 coronal mass ejection, *J. Geophys. Res.*, *114*, A10102, doi:10.1029/2009JA014167.

1. Introduction

[2] It has been one of the most fundamental topics in the field of Sun-Earth connection and space weather research to understand the generation mechanism of a southward pointing interplanetary magnetic field (IMF) at the Earth, since geomagnetic storms were found to be caused by prolonged, large-amplitude, and southward pointing IMF [Gonzalez and Tsurutani, 1987]. Coronal mass ejections (CMEs) and corotating interaction regions (CIRs) are the two major large-scale solar wind structures capable of producing such a geoeffective IMF [e.g., Kataoka and Miyoshi, 2006]. Comprehensive observations of the Sun and solar wind during solar cycle 23 enabled us to confirm that the major cause of large geomagnetic storms is the large-amplitude IMF associated with CMEs [Zhang *et al.*, 2007] and relatively small geomagnetic storms are caused by the southward IMF associated with CIRs [Richardson *et al.*, 2006].

[3] The magnetic cloud [Burlaga *et al.*, 1981] is a subset of CME-related IMF structures, characterized by low proton temperature, enhanced IMF amplitude, and slow rotation of IMF directions through a large angle [Klein and Burlaga, 1982]. The southward pointing IMF within the magnetic clouds usually satisfies the driving condition of geomagnetic

storms. On the basis of the low β property, magnetic clouds have been approximated by several types of force-free fields, such as a cylindrical flux rope [Goldstein, 1983; Marubashi, 1986], torus-shaped flux rope [Marubashi and Lepping, 2007], or spheroidals [Vandas *et al.*, 1993a, 1993b]. CME-driven geomagnetic storms are caused not only by magnetic clouds but also by many different types of CME-related IMF structures, such as the IMF compressed by interplanetary shock waves located ahead of high-speed CMEs [Tsurutani and Gonzalez, 1997], and/or draped IMF created by the propagation of CMEs in the ambient solar wind [Gosling and McComas, 1987; McComas *et al.*, 1989; Watari *et al.*, 2004; Liu *et al.*, 2008].

[4] Magnetohydrodynamics (MHD) [Alfvén, 1942] is the fundamental physics for describing the global evolution of the solar wind and IMF [see Parker, 2007]. Three-dimensional MHD simulation is necessary to fully understand the dynamic variation of the complicated IMF structures associated with CMEs. A number of 3-D MHD simulations of the solar wind have been performed during the last decade to investigate the basic evolution and propagation of several types of CMEs, such as the time-dependent pulse [Odstrcil and Pizzo, 1999; Odstrcil *et al.*, 2004; Hayashi *et al.*, 2006; Shen *et al.*, 2007; Wu *et al.*, 2007], the toroidal flux rope [Vandas *et al.*, 2002], the simulated flux rope [Manchester *et al.*, 2004a, 2004b], or the spheromak [Vandas *et al.*, 1997, 1998]. The ambient solar wind used in their simulations are either uniform [Vandas *et al.*, 1997, 1998, 2002], structured [Odstrcil and Pizzo, 1999; Manchester *et al.*, 2004a, 2004b], or realistic [Odstrcil *et al.*, 2004; Hayashi *et al.*, 2006; Shen *et al.*, 2007; Wu *et al.*, 2007]. A self-consistent modeling of the 3-D propagation of a magnetic cloud in a realistic ambient solar wind remains a challenging problem.

[5] Integrated frameworks connecting the models of solar corona, ejecta, and solar wind have been developed [e.g.,

¹Advanced Science Institute, Institute of Physics and Chemical Research, Wako, Japan.

²Interactive Research Center of Science, Tokyo Institute of Technology, Meguro, Japan.

³Institute for Research on Earth Evolution, Japan Agency for Marine-Earth Science and Technology, Yokosuka, Japan.

⁴Solar-Terrestrial Environment Laboratory, Nagoya University, Chikusa City, Japan.

⁵National Institute of Information and Communications Technology, Koganei, Japan.

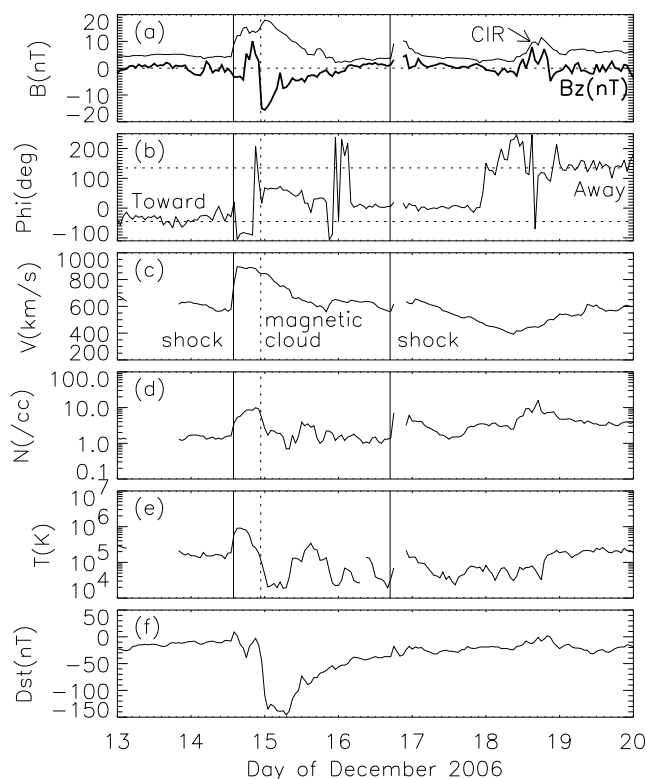


Figure 1. OMNI-2 solar wind and Dst profile for week of the 13 December 2006 coronal mass ejection (CME) event. From top to bottom, shown are (a) interplanetary magnetic field (IMF) amplitude and the GSE southward component (solid line), (b) IMF longitude in GSE coordinates, (c) solar wind speed, (d) number density, (e) proton temperature, and (f) Dst index.

Luhmann *et al.*, 2004; Tóth *et al.*, 2007]. However, it is still difficult to simultaneously reproduce the in situ observations of such basic solar wind structures as magnetic cloud, shock, and sheath. The purpose of this paper is to reproduce the interplanetary propagation of a magnetic cloud in a realistic ambient solar wind, using a newly developed 3-D MHD solar wind model named “MHD cube,” in order to understand the basic evolution of the magnetic cloud, interplanetary shock, and associated global IMF structures. We focus on a CME event of 13 December 2006, the last CME-driven large storm event during solar cycle 23. In section 2, we briefly review the CME event to raise a puzzling issue showing the coronagraph observation and in situ solar wind observation. In sections 3 and 4, we describe the MHD cube model to explain how to create the ambient solar wind and introduce a transient disturbance, respectively. In section 5, we compare the in situ solar wind observation and our modeling results to discuss the 3-D morphology of the CME evolution. In section 6, we summarize the results and discuss the capabilities and limitations of the MHD cube model.

2. The 13 December 2006 CME Event

[6] A high-speed halo-type CME was observed by Solar and Heliospheric Observatory (SOHO)/Large Angle and Spectrometric Coronagraph (LASCO) on 13 December

2006, associated with X3.4 flare at S06W23 (NOAA AR10930). The CME speed is estimated as 1774 km s^{-1} by Dr. S. Yashiro (http://cdaw.gsfc.nasa.gov/CME_list/). A large isolated CME-driven geomagnetic storm was observed on 14–15 December 2006. The provisional Dst index reached -146 nT at the storm peak, as shown in Figure 1f. This event is suitable for this study because HINODE data are fully available for diagnosing the detailed vector magnetic field of the active region.

[7] Figure 1 shows the solar wind profile at the Earth during the week of the CME event. OMNI-2 hourly data is obtained from the Web site (<http://omniweb.gsfc.nasa.gov/>). After the sudden arrival of an interplanetary shock on 14 December 2006, typical magnetic cloud properties are identified by the enhanced IMF, slow IMF rotation, and low temperature. The prolonged large-amplitude southward IMF exists within the magnetic cloud that caused the large geomagnetic storm. The magnetic cloud was embedded in toward IMF polarity, and a sector boundary arrived at the end of 17 December 2006, followed by a typical corotating interaction region on 18–19 December 2006. Another interplanetary shock associated with a different CME was observed on 16 December 2006.

[8] There are puzzling observations in the 13 December 2006 CME event. Using the Grad-Shafranov reconstruction technique of the magnetic cloud [Hau and Sonnerup, 1999; Hu and Sonnerup, 2002], Liu *et al.* [2008] suggested that the Earth passed near the center of an inclined north–south aligned flux rope. The initial propagation direction of the CME is, however, significantly westward and southward as shown in Figure 2. Assuming that the flux rope CME propagated significantly westward and southward, it is naturally expected that the Earth should pass the western edge of the flux rope, instead of the center of the flux rope. Understanding these observations in a simple scenario is therefore not straightforward, and this is an interesting challenge to address the 3-D MHD modeling.

3. MHD Solar Wind Model

[9] The time evolution of large-scale solar wind plasma and IMF follows MHD (see Parker [2007]). The ideal MHD

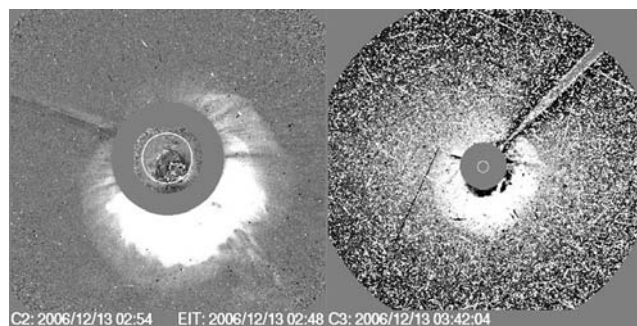


Figure 2. Coronagraph difference images of the 13 December 2006 CME as seen by Solar and Heliospheric Observatory (SOHO)/Large Angle and Spectrometric Coronagraph (LASCO) (left) C2 and (right) C3. White circles indicate the position of the Sun. The images are adapted from the LASCO CME Catalog at NASA/Goddard Space Flight Center.

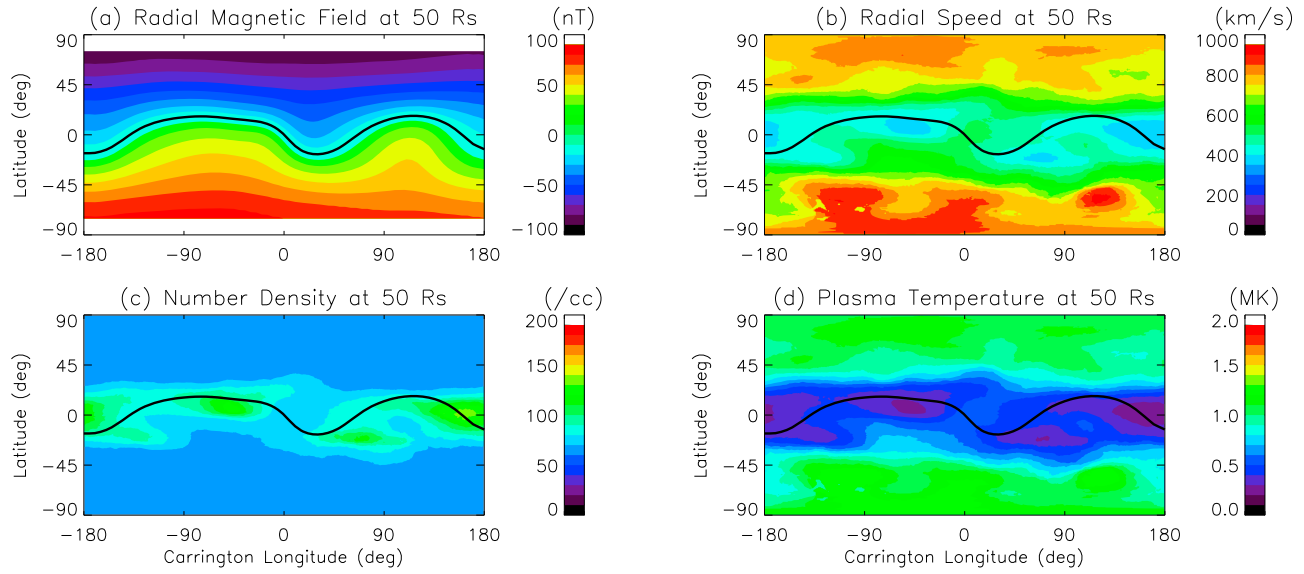


Figure 3. Inferred solar wind parameters at the inner boundary of $50 R_S$ sphere. (a) Radial magnetic field and (b) radial speed are based on Wilcox Solar Observatory and interplanetary scintillation observations of Solar-Terrestrial Environmental Laboratory, respectively. (c) Number density and (d) plasma temperature are empirically calculated as functions of the radial speed. Solid curves show the current sheet location of zero radial magnetic field.

equations to be solved in the conservation form are as follows,

$$\frac{\partial}{\partial t} \begin{pmatrix} \rho \\ \rho \mathbf{v} \\ e \\ \mathbf{B} \end{pmatrix} + \nabla \cdot \begin{pmatrix} \rho \mathbf{v} + p_t \mathbf{I} - \mathbf{B}\mathbf{B} \\ (e + p_t) \mathbf{v} - \mathbf{B}(\mathbf{B} \cdot \mathbf{v}) \\ \mathbf{v}\mathbf{B} - \mathbf{B}\mathbf{v} \end{pmatrix} = \begin{pmatrix} 0 \\ 0 \\ 0 \\ 0 \end{pmatrix}, \quad (1)$$

$$p_t = p + \frac{B^2}{2}, \quad e = \frac{\rho v^2}{2} + \frac{p}{\gamma - 1} + \frac{B^2}{2}, \quad (2)$$

where $\gamma = 5/3$ is the ratio of specific heat, and the basic quantities of ρ , \mathbf{v} , p , and \mathbf{B} represent normalized density, velocity, pressure, and magnetic field, respectively. The cell-centered Total Variation Diminishing (TVD) scheme [Harten and Hyman, 1983] with second-order MUSCL (Monotone Upstream-centered Schemes for Conservation Laws) method [Van Leer, 1979] is applied using the Harten-Lax-van Leer discontinuity (HLLD) approximate Riemann solver [Miyoshi and Kusano, 2005]. The HLLD method is excellent in terms of the positivity, simplicity, and efficiency [Stone et al., 2008], even comparing it to the most popular Roe method [Roe, 1981; Ryu and Jones, 1995]. The hyperbolic divergence cleaning technique of Dedner et al. [2002] is applied to remove numerically finite values of $\text{div } \mathbf{B}$.

[10] The numerical experiment is modeled as simply as possible. The simulation box consists of 256^3 uniform cubic cells, with the spatial resolution of 2.0 solar radii (R_S). The Sun is located at the center of the cubic simulation box at the origin $(x, y, z) = (0, 0, 0) R_S$, while the Earth is fixed at a position $(x, y, z) = (215, 0, 0) R_S$, where the z axis is parallel to the Sun's rotation axis. Free boundary condition is applied at the outer edges. Basic MHD quantities are inserted at a $50 R_S$ spherical surface as time-varying inner boundary to drive the supersonic and super Alfvénic solar wind flowing outward in radial direction from the Sun.

[11] Figure 3 shows the assumed ambient solar wind parameters at the inner boundary for the experiment of the 13 December 2006 CME event. The radial velocity map at a source surface of $2.5 R_S$ was obtained from the interplanetary scintillation (IPS) tomography method [Kojima et al., 1998], based on two months data starting from 1 October 2006. Solar-Terrestrial Environment Laboratory stopped the IPS observation at 7 December 2006 for wintering of antennas at the mountain areas. The two months period is the best time interval to obtain the whole velocity map without large data gaps by the tomography method, and it is also a quiet period during which the monthly velocity map does not change significantly in each Carrington map. Constant speed is assumed to map from the source surface to the inner boundary at $50 R_S$. The magnetic field at the source surface of $2.5 R_S$ is obtained from the Wilcox Solar Observatory's potential field model [Hoeksema et al., 1982], centering the 360° Carrington longitude of CR2050 on 14 November 2006. Centering at 14 November is consistent with the two month IPS observation. The result from the $2.5 R_S$ radial model is selected because of its simplicity. The radial magnetic field at the source surface B_s is scaled to the radial IMF B_r at $50 R_S$, assuming the decreasing strength with the square of distance. We further employ a simple power law modification of the boundary magnetic field to push the flux closer to the current sheet, creating a more uniform flux distribution away from the current sheet and a steeper gradient across the current sheet as follows,

$$B_r = 10(B_s)^{0.5} \left(\frac{2.5}{50} \right)^2, \quad (3)$$

where we select the power index of 0.5 for simplicity, and a factor of 10 is multiplied to adjust it to the actual IMF strength. A 14 deg eastward shift of the synoptic map is

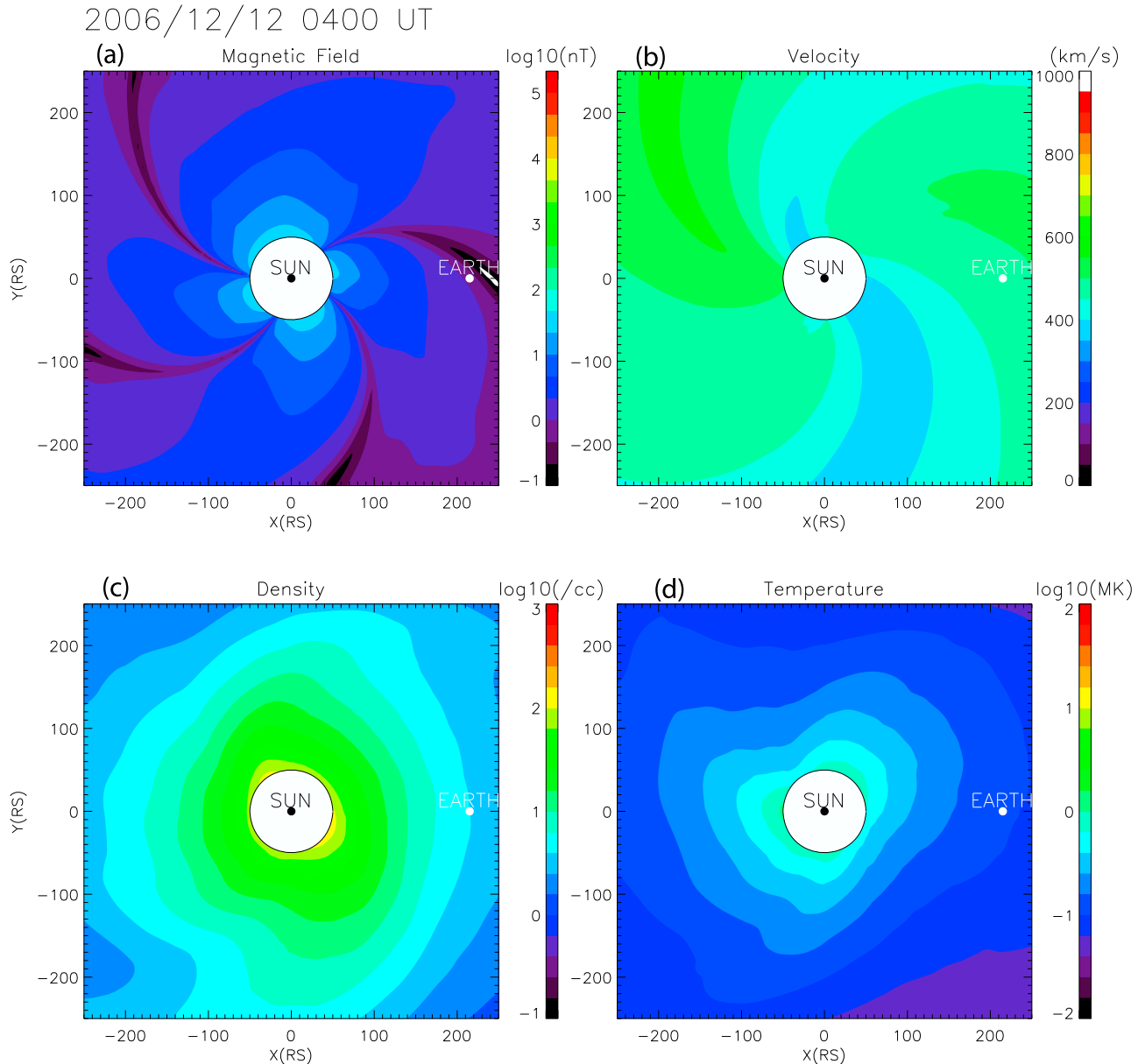


Figure 4. The ambient solar wind structure at 0400 UT on 12 December 2006. The amplitudes of MHD parameters are shown at the equatorial plane: (a) interplanetary magnetic field strength, (b) solar wind speed, (c) number density, and (d) plasma temperature.

further applied, considering the approximate travel time from the solar surface to 50 Rs with a constant speed of 400 km s^{-1} .

[12] Following the method of *Hayashi et al.* [2003], number density n and proton temperature T at 50 Rs distance are calculated as empirical functions of radial speed V as follows:

$$n = 62.98 + 866.4 \left(\frac{V}{100} - 1.549 \right)^{-3.402}, \quad (4)$$

$$T = -0.455 + 0.1943 \frac{V}{100}, \quad (5)$$

where the units are n [/cc], T [MK], and V [km s^{-1}]. The proton temperature is related to the MHD pressure using

the relation $p = 2nk_B T$, where k_B is the Boltzman constant. The inner boundary map is rotated against the z axis at $\Omega = 27.2753 \text{ day/rotation rate}$. The azimuth magnetic field B_ϕ is added finally as a function of radial speed to reproduce the Parker spiral:

$$\frac{B_\phi}{B_r} = \frac{R\Omega \sin \lambda}{V}, \quad (6)$$

where λ is the colatitude from the Z axis, and R is 50 Rs. We use a numerical relaxation technique to obtain the ambient solar wind by rotating the inner boundary for a week in advance, starting from the analytic solution of radial expansion flow with constant speed. Figure 4 shows the MHD

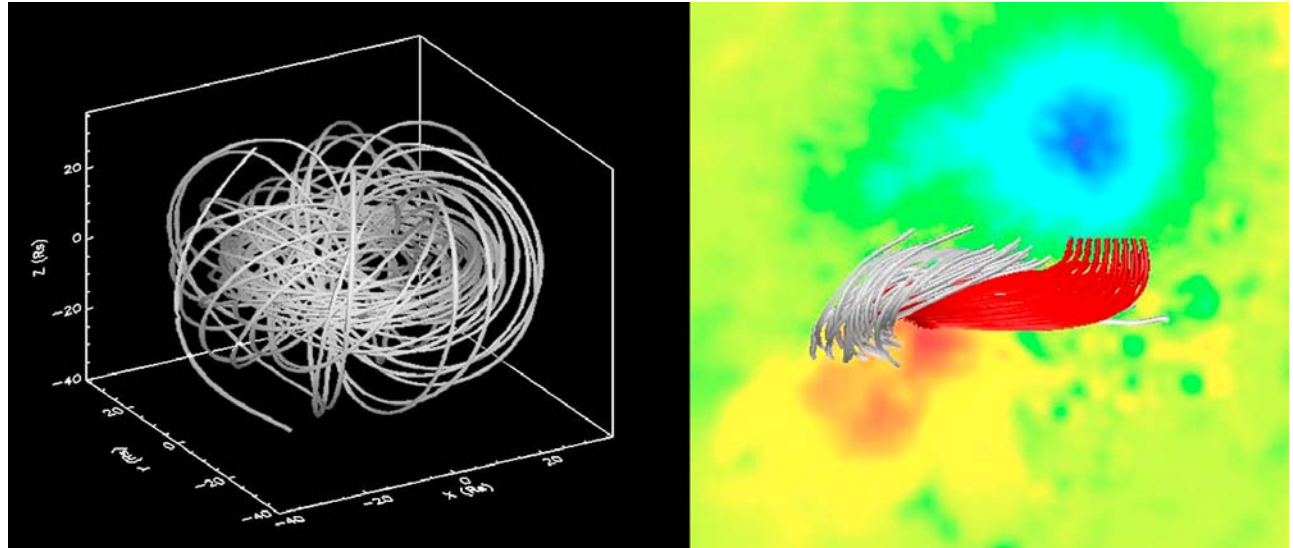


Figure 5. Magnetic field lines of (left) the spheromak and (right) the closed loop morphology of AR10930 computed using a nonlinear force-free (NLFF) model. The background contour shows positive (warm color) and negative (cold color) magnetic polarity of the photosphere. The red and white NLFF loops correspond to the toroidal and poloidal fields of spheromak, respectively. A similar left-handed magnetic field structure can be seen in both Figure 5 (left) and Figure 5 (right), where the toroidal fields direct roughly westward and the poloidal fields surround over the toroidal fields from south to north.

parameters of the obtained ambient solar wind at the equatorial plane at 0400 UT on 12 December 2006. Basic structures such as the Parker spiral, heliospheric current sheet, and corotating interaction regions are reproduced. The Earth recently entered a toward IMF sector region, and will pass a current sheet and corotating interaction region in a week, which is consistent with the observations of Figure 1.

4. Spheromak CME Model

[13] A spheromak-type magnetic field is introduced as the simplest CME model. The spheroidal magnetic field may be a natural product of a plasmoid ejected from a solar flare via reconnection [Gibson and Fan, 2008], although the actual existence in the solar wind is under debate [e.g., Vandas *et al.*, 1993a, 1993b, 2002; Farrugia *et al.*, 1995]. In this paper, the initial shape of the magnetic cloud is simply assumed to be a sphere with the radius a . The inner magnetic field configuration is assumed to be the spheromak of Chandrasekhar and Kendall [1957]:

$$B_r = 2B_0 \frac{j_1(\alpha r)}{\alpha r} \cos(\theta), \quad (7)$$

$$B_\theta = -B_0 (j_1(\alpha r) + \alpha r j_1'(\alpha r)) \sin(\theta), \quad (8)$$

$$B_\phi = B_0 j_1(\alpha r) \sin(\theta), \quad (9)$$

where the polar coordinate system (r, θ, ϕ) is defined by the polar axis of the spheromak, $\alpha = 4.493409458a^{-1}$ is the constant derived from the force-free condition of $\nabla \times \mathbf{B} = \alpha \mathbf{B}$ with the boundary condition of $B_r = 0$ at $r = a$. The parameter

α becomes negative for left-handed polarity. The spherical Bessel function and the derivative are

$$j_1(x) = \frac{\sin x - x \cos x}{x^2}, \quad (10)$$

$$j_1'(x) = \frac{2x \cos x + (x^2 - 2) \sin x}{x^2}. \quad (11)$$

[14] The magnetic helicity H in a spheromak is computed as

$$H = \alpha^{-1} \int_0^{2\pi} d\phi \int_0^\pi d\theta \int_0^a r^2 dr \sin \theta B^2 = 0.0454a^4 B_0^2. \quad (12)$$

A realistic magnetic helicity can be estimated from HINODE observations using the local correlation tracking method coupled with induction equations [Kusano *et al.*, 2002] to obtain the rough estimate of $B_0 = 10^{14} a^{-2}$ T for AR10930. We analyzed SOT/SP data obtained during December 9–13 during which the observed time intervals were 1–5 h. The magnetic field B_0 estimates the upper bounds. The model constraints are B_0 and the polar axis of spheromak, and they would be useful for making predictions because B_0 varies event to event. In fact, there is a correlation between the magnetic parameters and flare activity [Yamamoto and Sakurai, 2009]. The nonlinear force-free method [Inoue *et al.*, 2008] based on the HINODE observations also gives another independent estimation of H in the same order of magnitude. An illustration of the 3-D magnetic field configuration of the spheromak is shown in Figure 5 (left), comparing it with the nonlinear force-free (NLFF) field (Figure 5, right) based on the HINODE observation. A similar left-handed magnetic

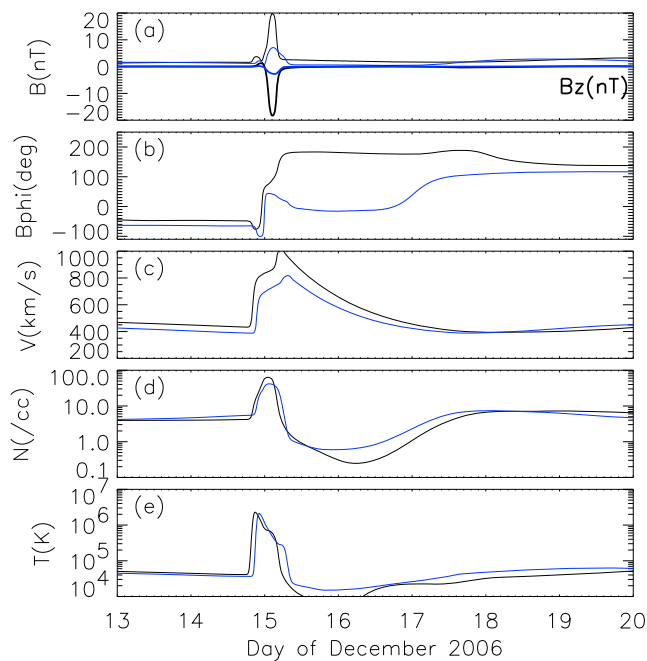


Figure 6. Simulated solar wind profile at the Earth for the week of the 13 December 2006 CME event. From top to bottom, shown are (a) IMF amplitude and the GSE southward component (solid line), (b) IMF longitude in GSE coordinates, (c) solar wind speed, (d) number density, and (e) plasma temperature. Blue lines show the solar wind profile computed at a position 15 deg westward of the Earth.

field structure can be seen in both Figure 5 (left) and Figure 5 (right), where the toroidal fields direct roughly westward and the poroidal fields surround over the toroidal fields from south to north.

[15] MHD quantities at the inner boundary are perturbed in a specified way as the spheroidal magnetic cloud moves across the computational boundary. In this paper we deliberately choose the parameters to provide the best possible results from this model. The magnetic field of the spheromak is introduced by simply superposing it on the ambient field to avoid any artificial $\text{div } \mathbf{B}$ problems. The radial speed V_{r0} inside the cloud is assumed to be constant, where the transit time τ is directly related to the radius as $\tau = 2a/V_{r0}$, where the radius is assumed as $a = 30 R_S$. The spheromak is covered by a concentric spherical transition region where the speed smoothly decreases to the ambient level at the radius of $40 R_S$ using a trigonometric function of \cos^2 . SOHO/LASCO observed that the CME reached $6 R_S$ at 0300 UT (Figure 2). Assuming a constant deceleration of the CME speed from 1800 km s^{-1} at $6 R_S$ to 1000 km s^{-1} at $50 R_S$, the CME arrival time at $50 R_S$ is roughly estimated to be 0900 UT. The density and temperature inside the magnetic cloud are assumed to be twice that of the ambient solar wind. The ejection direction of the magnetic cloud is assumed to be 15 deg westward and 15 deg southward from the Sun-Earth line, roughly consistent with the coronagraph observations in Figure 2. The polar axis of the ejected spheromak is assumed to be rotated 90 deg toward the positive Y direction to find a better agreement with the in situ IMF observations, although the original polar axis at the lower corona mostly parallel to local north, which

seems to be consistent with the HINODE observations (Figure 5). We discuss the need and the meaning of this ad hoc optimization process of arbitrary rotation in section 5.

5. Results and Discussions

[16] Figure 6 shows a simulated solar wind profile at the virtual Earth position for the same time interval of a week, using the same vertical scale as Figure 1. To see a possible range of variations at the 1 AU in situ sampling, the simulated solar wind profile approximately 15 deg westward of the Earth is also shown by blue lines. The most important point in Figure 6 is the quantitative reproduction of the southward Bz using the spheromak CME model. Many other basic structures are also reasonably reproduced as follows: The interplanetary shock arrived at 1900 UT on 14 December 2006, which is 5 hours later than the actual arrival. The interplanetary shock and magnetic cloud arrived in the toward IMF polarity before a current sheet arrival, followed by a corotating interaction region on 18–19 December 2006 as observed in Figure 1, although the CIR structures is much fainter in the model result. The rarefaction structure is also reproduced as identified by the monotonic speed decrease with density rarefaction, although significant perturbations coexist to disturb the actual rarefaction profile in Figure 1. Predicting the rarefaction structure is important for forecasting space weather of terrestrial radiation belt. In fact, during the storm recovery phase of this December 2006 storm, the radiation belt electron flux was greatly enhanced during the rarefaction phase because of the “double rarefaction” mechanism [Kataoka and Miyoshi, 2008a, 2008b].

[17] The simulated solar wind profile in Figure 6 is obtained by rotating the polar axis of the ejected spheromak by 90 deg anticlockwise, to see a better agreement with the in situ observation of the IMF. The in situ magnetic field rotation inside the magnetic cloud does not show a good agreement if the polar axis of the spheromak is parallel to local north. This result may imply existence of a significant anticlockwise writhe from the initial configuration occurring below $50 R_S$, possibly below the coronal height where the magnetic field force dominates. The rotation of the magnetic field vector at 1 AU associated with the spheromak CME is sensitive to the initial magnetic field configuration at the inner boundary and does not change significantly during the propagation, because of relatively small magnetic force. The amount of rotation of the field vector is also sensitive to which part of the magnetic structure passes by the observer (thus the magnetic cloud trajectory), and a smaller magnetic cloud is therefore more sensitive to this effect. The arrival time of the interplanetary shock and/or magnetic cloud is earlier in case of high cloud density, because of the large total momentum against the obstacle of slow ambient solar wind. A systematic parameter survey using the MHD cube model to understand such sensitivities to various initial conditions is beyond the scope of this paper and remains a future work.

[18] The basic structures such as magnetic cloud, shock, and sheath are investigated in more detail for the rotated spheromak. Figure 7 shows the expanded view of velocity and magnetic field vectors in GSE coordinates at the Earth position for two days. The time resolutions for the ACE magnetic field and velocity observations are 16 s and 64 s,

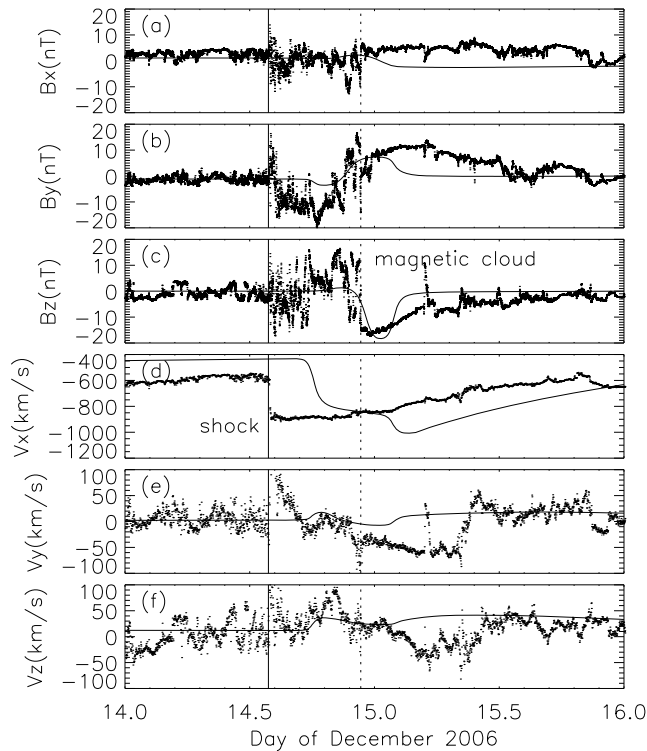


Figure 7. Simulated solar wind profile at the Earth for the time interval from 14 to 16 December 2006. We add 2 h to the time axis of simulated profiles for a better comparison. From top to bottom, shown are three components of (a, b, c) interplanetary magnetic field and (d, e, f) solar wind velocity in GSE coordinates. The ACE observations are shown by dots. Vertical solid lines show the interplanetary shock arrival, and vertical dotted lines show the beginning of the magnetic cloud.

respectively. We add 2 hours to the time axis of simulated profiles just for a better comparison of the IMF rotation's turning from north to south (from positive Z_{GSE} to negative Z_{GSE}). The flow direction inside the magnetic cloud is westward (negative Y_{GSE}), as expected from the bulk motion of CME, while the flow deflection just after the shock arrival is eastward (positive Y_{GSE}) and northward (positive Z_{GSE}) in both simulations and observations, as naturally expected from the 3-D shock geometry [e.g., Kataoka *et al.*, 2005].

[19] One of the most useful properties of MHD is the ability to track the same magnetic field lines in order to understand the time evolution of the 3-D morphology. Figure 8 shows the time evolution of the same magnetic field lines initially located inside of the spheromak. By definition, spheromaks are magnetically closed structures fully detached from the Sun. For example, Vandas *et al.* [1997, 1998] have shown that a spheroid with its polar axis parallel to the ambient evolves into a body similar to a toroid during propagation in the solar wind. In our simulation, on the contrary, most of the magnetic field lines of spheromak CME are connected to the inner boundary from the beginning, as shown in Figure 8, since the magnetic field of the spheromak is introduced by simple superposition on the ambient field. In fact, the IMF connection between the Sun

and Earth is implied within the magnetic cloud from electron SEP observations [Liu *et al.*, 2008]. During CME propagation, the overall morphology is elongated perpendicularly to the radial direction, keeping the sense of the IMF rotations of the spheromak. The meridional and azimuthal extent does not change much during the propagation and is almost defined by the initial size of the spheromak. Under the same conditions of initial helicity and magnetic flux, the basic propagation processes are not sensitive to the size of the spheromak. From Figure 8, it is found that the Earth's trajectory across an eastern shoulder of the deformed spheromak can explain both the result of Liu *et al.* [2008] and the coronagraph observations described in section 2. The eastern shoulder trajectory should be observed as central passage of a flux rope at in situ measurement, and the whole spheromak structure propagate southward and westward as it appeared in the coronagraph.

6. Summary

[20] The MHD cube model was developed to reconstruct the interplanetary propagation of CME on 13 December 2006 in a realistic ambient solar wind. The magnetic cloud and associated structures, such as shock and sheath, are reasonably explained by the westward and southward propagation of a spheromak CME. Consequently, the spheromak CME model is topologically complex enough to be consistent with in situ observations, such as southward IMF associated with CMEs. Introducing the 3-D spheromak-type CME magnetic field is a new approach in this paper, while it is possible to implement the spheromak CME in other MHD models, and the expected results should not be significantly different depending on different models.

[21] The MHD cube is the simplest model of the dynamic solar wind, and free from a lot of problems in complicated grid systems. The uniform resolution makes the analysis simple, and provides a good starting point for further development such as data assimilation and adaptive mesh refinement (AMR) technique. The uniform resolution of $2 R_{\text{S}}$ is coarse at the inner edge, and fine at 1 AU, which will be naturally improved by the AMR technique. The inner boundary can be replaced by some other solar wind models or observations as desired in the future. The tunable free parameters of the spheromak CME model would be the initial speed, width (size of spheromak), and direction, which are related to observable quantities from a coronagraph. Further, detailed solar magnetograms, if available, can produce a possible restriction in the polar axis and helicity of the spheromak.

[22] Limitations also exist. Odstroil and Pizzo [1999] suggested that initial CME position relative to the current sheet is important for taking into account the interaction between CMEs and the slow wind. A dynamic MHD coronal model is needed to address such interactions and the initial evolution of CMEs and associated shock formations across the critical point of solar wind acceleration. In fact, it has been suggested that the initial CME evolution and shock formation significantly depend on the coronal heating model [Jacobs *et al.*, 2005]. As members of a multi-institute collaboration of the space-weather-modeling taskforce in Japan [Shibata and Kamide, 2007] that is working to solve such remaining problems, we are developing an integrated framework to

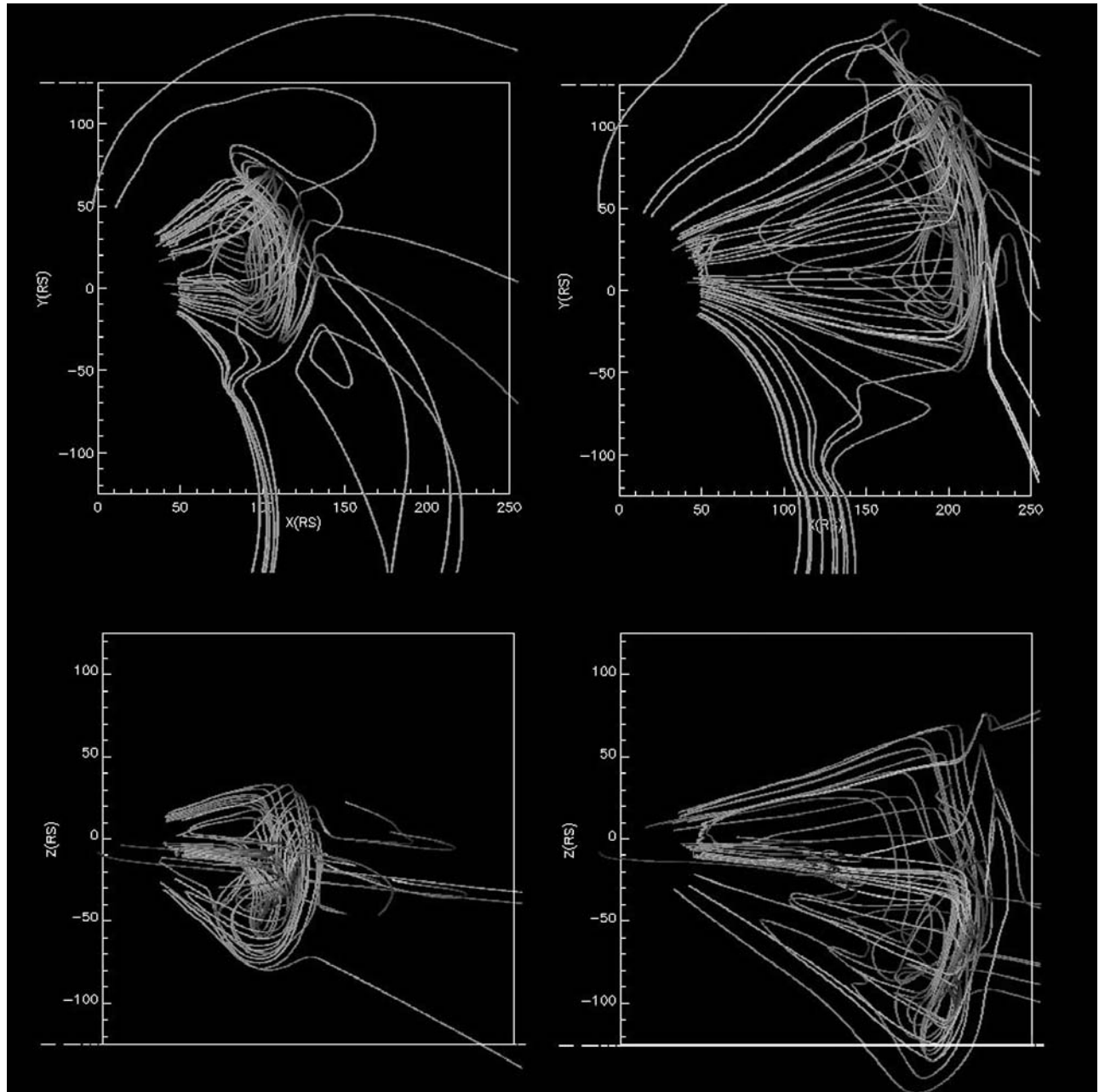


Figure 8. Time evolution of the same magnetic field lines inside spheromak CME at (left) 0400 UT on 13 December 2006 and (right) 0400 UT on 14 December 2006. (top) View from the north (XY plane). (bottom) View from the east (YZ plane). The Sun is located at the origin, and the Earth is located at $(X, Y, Z) = (215, 0, 0)$.

initiate the CME from the solar surface based on HINODE observations for creating more realistic CME structures. The initial results of our integrated framework will be shown elsewhere.

[23] **Acknowledgments.** The code development of the MHD cube by R.K. owes thanks to ACT-JST Summer Seminar of Astrophysical Plasma Simulation held by R. Matsumoto in 2003. R.K. thanks K. Tomisaka, T. Hanawa, and T. Yokoyama for their teaching how to develop an MHD code in the Summer Seminar. R.K. thanks T. Miyoshi of Hiroshima University for his practical advice on the HLLD method. The CME catalog is generated and maintained at the CDAW Data Center by NASA and the Catholic University of America in cooperation with the Naval Research Laboratory. SOHO is a project of international cooperation between ESA

and NASA. The solar magnetic field data is obtained from the Wilcox Solar Observatory. The OMNI-2 and ACE solar wind data are provided from NASA/NSSDC. The *Dst* index is provided from Kyoto University. Hinode is a Japanese mission developed and launched by ISAS/JAXA, with NAOJ as domestic partner and NASA and STFC (UK) as international partners. It is operated by these agencies in cooperation with ESA and NSC (Norway). The work by R.K. was supported by a research fellowship of Special Postdoctoral Research Program at RIKEN. R.K. thanks the RIKEN Super Combined Cluster (RSCC) and Nagoya University in collaboration with STEL for computational resources. This work was supported by the Grant-in-Aid for Creative Scientific Research (20740286) and “The Basic Study of Space Weather Prediction” (17GS0208, Head Investigator: K. Shibata) from the Ministry of Education, Science, Sports, Technology, and Culture of Japan.

[24] Amitava Bhattacharjee thanks Sarah Gibson and another reviewer for their assistance in evaluating this paper.

References

- Alfvén, H. (1942), Existence of electromagnetic-hydrodynamic waves, *Nature*, *150*, 405–406, doi:10.1038/150405d0.
- Burlaga, L. F., E. Sittler, F. Mariani, and R. Schwenn (1981), Magnetic loop behind an interplanetary shock, *J. Geophys. Res.*, *86*, 6673–6684, doi:10.1029/JA086iA08p06673.
- Chandrasekhar, S., and P. C. Kendall (1957), On force-free magnetic fields, *Astrophys. J.*, *126*, 457–460, doi:10.1086/146413.
- Dedner, A., F. Kemm, D. Kroner, C.-D. Munz, T. Schnizer, and M. Wessberg (2002), Hyperbolic divergence cleaning for the MHD equations, *J. Comput. Phys.*, *175*, 645–673, doi:10.1006/jcph.2001.6961.
- Farrugia, C. J., V. A. Osherovich, and L. F. Burlaga (1995), Magnetic flux rope versus the spheromak as models for interplanetary magnetic clouds, *J. Geophys. Res.*, *100*, 12,293–12,306, doi:10.1029/95JA000272.
- Gibson, S. E., and Y. Fan (2008), Partially ejected flux ropes: Implications for interplanetary coronal mass ejections, *J. Geophys. Res.*, *113*, A09103, doi:10.1029/2008JA013151.
- Goldstein, H. (1983), On the field configuration in magnetic clouds, in *Solar Wind Five*, edited by M. Neugebauer, pp. 731–733, NASA, Washington, D. C.
- Gonzalez, W. D., and B. T. Tsurutani (1987), Criteria of interplanetary parameters causing intense magnetic storms ($Dst < -100$ nT), *Planet. Space Sci.*, *35*, 1101–1109, doi:10.1016/0032-0633(87)90015-8.
- Gosling, J. T., and D. J. McComas (1987), Field line draping about fast coronal mass ejecta: A source of strong out-of-ecliptic interplanetary magnetic fields, *Geophys. Res. Lett.*, *14*, 355–358, doi:10.1029/GL014i004p00355.
- Harten, A., and J. M. Hyman (1983), Self adjusting grid methods for one-dimensional hyperbolic conservation laws, *J. Comput. Phys.*, *50*, 235, doi:10.1016/0021-9991(83)90066-9.
- Hau, L.-N., and B. Sonnerup (1999), Two-dimensional coherent structures in the magnetopause: Recovery of static equilibria from single-spacecraft data, *J. Geophys. Res.*, *104*, 6899–6917, doi:10.1029/1999JA900002.
- Hayashi, K., M. Kojima, M. Tokumaru, and K. Fujiki (2003), MHD tomography using interplanetary scintillation measurement, *J. Geophys. Res.*, *108*(A3), 1102, doi:10.1029/2002JA009567.
- Hayashi, K., X. P. Zhao, and Y. Liu (2006), MHD simulation of two successive interplanetary disturbances driven by cone-model parameters in IPS-based solar wind, *Geophys. Res. Lett.*, *33*, L20103, doi:10.1029/2006GL027408.
- Hoeksema, J. T., J. M. Wilcox, and P. H. Scherrer (1982), Structure of the heliospheric current sheet in the early portion of sunspot cycle 21, *J. Geophys. Res.*, *87*, 10,331–10,338, doi:10.1029/JA087iA12p10331.
- Hu, Q., and B. U. Ö. Sonnerup (2002), Reconstruction of magnetic clouds in the solar wind: Orientations and configurations, *J. Geophys. Res.*, *107*(A7), 1142, doi:10.1029/2001JA000293.
- Inoue, S., K. Kusano, S. Masuda, T. Miyoshi, T. T. Yamamoto, T. Magara, S. Tsuneta, T. Sakurai, and T. Yokoyama (2008), Three-dimensional structure analysis of coronal magnetic field in AR NOAA 10930 based on vector magnetogram observations with Hinode/SOT, *First Results From Hinode ASP Conference Series*, vol. 397, pp. 110–113, edited by S. A. Matthews, J. M. Davis, and L. K. Harra, Astronomical Society of the Pacific Trinity College, Dublin.
- Jacobs, C., S. Poedts, B. Van der Holst, and E. Chane (2005), On the effect of the background wind on the evolution of interplanetary shock waves, *Astron. Astrophys.*, *430*, 1099–1107, doi:10.1051/0004-6361/20041676.
- Kataoka, R., and Y. Miyoshi (2006), Flux enhancement of radiation belt electrons during geomagnetic storms driven by coronal mass ejections and corotating interaction regions, *Space Weather*, *4*, S09004, doi:10.1029/2005SW000211.
- Kataoka, R., and Y. Miyoshi (2008a), Magnetosphere inflation during the recovery phase of geomagnetic storms as an excellent magnetic confinement of killer electrons, *Geophys. Res. Lett.*, *35*, L06S09, doi:10.1029/2007GL031842.
- Kataoka, R., and Y. Miyoshi (2008b), Average profiles of the solar wind and outer radiation belt during the extreme flux enhancement of relativistic electrons at geosynchronous orbit, *Ann. Geophys.*, *26*, 1335–1339.
- Kataoka, R., S. Watari, N. Shimada, H. Shimazu, and K. Marubashi (2005), Downstream structures of interplanetary fast shocks associated with coronal mass ejections, *Geophys. Res. Lett.*, *32*, L12103, doi:10.1029/2005GL022777.
- Klein, L. W., and L. F. Burlaga (1982), Interplanetary magnetic clouds at 1 AU, *J. Geophys. Res.*, *87*, 613–624, doi:10.1029/JA087iA02p00613.
- Kojima, M., M. Tokumaru, H. Watanabe, A. Yokobe, K. Asai, B. V. Jackson, and P. L. Hick (1998), Heliospheric tomography using interplanetary scintillation observations 2. Latitude and heliocentric distance dependence, *J. Geophys. Res.*, *103*, 1981–1989, doi:10.1029/97JA02162.
- Kusano, K., T. Maeshiro, T. Yokoyama, and T. Sakurai (2002), Measurement of magnetic helicity injection and free energy loading into the solar corona, *Astrophys. J.*, *577*, 501–512, doi:10.1086/342171.
- Liu, Y., J. G. Luhmann, P. C. Schroeder, L. Wang, Y. Li, R. P. Lin, S. D. Bale, R. Müller-Mellin, M. H. Acuña, and J.-A. Sauvaud (2008), A comprehensive view of the 13 December 2006 CME: From the Sun to interplanetary space, *Astrophys. J.*, *689*, 563–571, doi:10.1086/592031.
- Luhmann, J. G., S. C. Solomon, J. A. Linker, J. G. Lyon, Z. Mikic, D. Odstrcil, W. Wang, and M. Willberger (2004), Coupled model simulation of a Sun-to-Earth space weather event, *J. Atmos. Sol. Terr. Phys.*, *66*, 1243–1256, doi:10.1016/j.jastp.2004.04.005.
- Manchester, W. B., IV, T. I. Gombosi, I. Roussev, D. L. De Zeeuw, I. V. Sokolov, K. G. Powell, and G. Tóth (2004a), Three-dimensional MHD simulation of a flux rope driven CME, *J. Geophys. Res.*, *109*, A01102, doi:10.1029/2002JA009672.
- Manchester, W. B., IV, T. I. Gombosi, I. Roussev, A. Ridley, D. L. De Zeeuw, I. V. Sokolov, K. G. Powell, and G. Tóth (2004b), Modeling a space weather event from the Sun to the Earth: CME generation and interplanetary propagation, *J. Geophys. Res.*, *109*, A02107, doi:10.1029/2003JA010150.
- Marubashi, K. (1986), Structure of the interplanetary magnetic clouds and their solar origins, *Adv. Space Res.*, *6*(6), 335–338, doi:10.1016/0273-1177(86)90172-9.
- Marubashi, K., and R. P. Lepping (2007), Long-duration magnetic clouds: A comparison of analyses using torus- and cylinder-shaped flux rope models, *Ann. Geophys.*, *25*, 2453–2477.
- McComas, D. J., J. T. Gosling, S. J. Bame, E. J. Smith, and H. V. Cane (1989), A test of magnetic field draping induced BZ perturbations ahead of fast coronal mass ejecta, *J. Geophys. Res.*, *94*, 1465–1471, doi:10.1029/JA094iA02p01465.
- Miyoshi, T., and K. Kusano (2005), A multi-state HLL approximate Riemann solver for ideal magnetohydrodynamics, *J. Comput. Phys.*, *208*, 315–344, doi:10.1016/j.jcp.2005.02.017.
- Odstrcil, D., and V. J. Pizzo (1999), Distortion of the interplanetary magnetic field by three-dimensional propagation of coronal mass ejections in a structured solar wind, *J. Geophys. Res.*, *104*, 28,225–28,239, doi:10.1029/1999JA900319.
- Odstrcil, D., P. Riley, and X. P. Zhao (2004), Numerical simulation of the 12 May 1997 interplanetary CME event, *J. Geophys. Res.*, *109*, A02116, doi:10.1029/2003JA010135.
- Parker, E. N. (2007), *Conversations on Electric and Magnetic Fields in the Cosmos*, Princeton Series in Astrophysics, Princeton Univ. Press, Princeton, New Jersey.
- Richardson, I. G., et al. (2006), Major geomagnetic storms ($Dst \leq -100$ nT) generated by corotating interaction regions, *J. Geophys. Res.*, *111*, A07S09, doi:10.1029/2005JA011476.
- Roe, P. L. (1981), Approximate Riemann solvers, parameter vectors, and difference schemes, *J. Comput. Phys.*, *43*, 357, doi:10.1016/0021-9991(81)90128-5.
- Ryu, D., and T. W. Jones (1995), Numerical magnetohydrodynamics in astrophysics: Algorithm and tests for one-dimensional flow, *Astrophys. J.*, *442*, 228, doi:10.1086/175437.
- Shen, F., X. Feng, S. T. Wu, and C. Xiang (2007), Three-dimensional MHD simulation of CMEs in three-dimensional background solar wind with self-consistent structure on the source surface as input: Numerical simulation of the January 1997 Sun-Earth connection event, *J. Geophys. Res.*, *112*, A06109, doi:10.1029/2006JA012164.
- Shibata, K., and Y. Kamide (2007), Basic study of space weather predictions: A new project in Japan, *Space Weather*, *5*, S12006, doi:10.1029/2006SW000306.
- Stone, J. M., T. A. Gardiner, P. Teuben, J. F. Hawley, and J. B. Simon (2008), ATHENA: A new code for astrophysical MHD, *Astrophys. J. Suppl.*, *178*, 137–177.
- Tóth, G., D. L. De Zeeuw, T. I. Gombosi, W. B. Manchester, A. J. Ridley, I. V. Sokolov, and I. I. Roussev (2007), Sun-to-thermosphere simulation of the 28–30 October 2003 storm with the Space Weather Modeling Framework, *Space Weather*, *5*, S06003, doi:10.1029/2006SW000272.
- Tsurutani, B. T., and W. D. Gonzalez (1997), The interplanetary causes of magnetic storms: A review, in *Magnetic Storms*, *Geophys. Monogr. Ser.*, vol. 98, edited by B. T. Tsurutani et al., pp. 77–89, AGU, Washington, D. C.
- Van Leer, B. (1979), Towards the ultimate conservative difference scheme, V. A second-order sequel to Godunov's method, *J. Comput. Phys.*, *32*, 101–136, doi:10.1016/0021-9991(79)90145-1.
- Vandas, M., S. Fischer, P. Pelant, and A. Geranos (1993a), Spheroidal models of magnetic clouds and their comparison with spacecraft measurements, *J. Geophys. Res.*, *98*, 11,467–11,475, doi:10.1029/93JA00055.
- Vandas, M., S. Fischer, P. Pelant, and A. Geranos (1993b), Evidence for a spheroidal structure of magnetic clouds, *J. Geophys. Res.*, *98*, 21,061–21,069, doi:10.1029/93JA01749.
- Vandas, M., S. Fischer, P. Pelant, M. Dryer, Z. Smith, and T. Detman (1997), Propagation of a spheromak 1. Some comparisons of cylindrical

- and spherical magnetic clouds, *J. Geophys. Res.*, *102*, 24,183–24,193, doi:10.1029/97JA02257.
- Vandas, M., S. Fischer, M. Dryer, Z. Smith, and T. Detman (1998), Propagation of a spheromak 2. Three-dimensional structure of a spheromak, *J. Geophys. Res.*, *103*, 23,717–23,725, doi:10.1029/98JA01902.
- Vandas, M., D. Odstrcil, and S. Watari (2002), Three-dimensional MHD simulation of a loop-like magnetic cloud in the solar wind, *J. Geophys. Res.*, *107*(A9), 1236, doi:10.1029/2001JA005068.
- Watari, S., M. Vandas, and T. Watanabe (2004), Formation of a strong southward IMF near the solar maximum of cycle 23, *Ann. Geophys.*, *22*, 673–687.
- Wu, C.-C., C. D. Fry, S. T. Wu, M. Dryer, and K. Liou (2007), Three-dimensional global simulation of interplanetary coronal mass ejection propagation from the Sun to the heliosphere: Solar event of 12 May 1997, *J. Geophys. Res.*, *112*, A09104, doi:10.1029/2006JA012211.
- Yamamoto, T. T., and T. Sakurai (2009), Correlations between flare parameters and magnetic parameters in solar flares, *Publ. Astron. Soc. Jpn.*, *61*(1), 75–84.
- Zhang, J., et al. (2007), Solar and interplanetary sources of major geomagnetic storms ($Dst \leq -100$ nT) during 1996–2005, *J. Geophys. Res.*, *112*, A10102, doi:10.1029/2007JA012321.

T. Ebisuzaki, Advanced Science Institute, RIKEN, 2-1 Hirosawa, Wako, Saitama 351-0198 Japan.

S. Inoue, National Institute of Information and Communications Technology, 4-2-1 Nukui-Kitamachi, Koganei, Tokyo 184-8795, Japan.

R. Kataoka, Interactive Research Center of Science, Tokyo Institute of Technology, 2-12-1 Ookayama, Meguro-ku, Tokyo 152-8550, Japan.

D. Shiota, IFREE, JAMSTEC, 2-15 Natsushima-Cho, Yokosuka, Kanagawa 237-0061, Japan.

K. Kusano, M. Tokumaru, and T. T. Yamamoto, Solar-Terrestrial Environment Laboratory, Nagoya University, Furo-Cho, Chikusa-ku, Nagoya 464-8601, Japan.